

Unusual Spin Polarization in the Chirality Induced Spin Selectivity

Yotam Wolf,¹ Yizhou Liu,¹ Jiewen Xiao,¹ Noejung Park,² and Binghai Yan^{1,*}

¹*Department of Condensed Matter Physics, Weizmann Institute of Science, Rehovot 7610001, Israel*

²*Department of Physics, Ulsan National Institute of Science and Technology (UNIST), Ulsan, 44919 Republic of Korea*

(Dated: August 2, 2022)

Chirality-induced spin selectivity (CISS) refers to the fact that electrons get spin polarized after passing through organic chiral molecules in a nanoscale device. In CISS, chiral molecules are commonly believed to be a spin filter through which one favored spin transmits and the opposite spin gets reflected, i.e., transmitted and reflected electrons exhibit opposite spin polarization. In this work, we point out that such a spin filter scenario contradicts the principle that equilibrium spin current must vanish. Instead, we find that both transmitted and reflected electrons present the same type spin polarization, which is actually ubiquitous for a two-terminal device. More accurately, chiral molecules play the role of a spin polarizer rather than a spin filter. The direction of spin polarization is determined by the molecule chirality and the electron incident direction. And the magnitude of spin polarization relies on local spin-orbit coupling in the device. Our work brings a deeper understanding on CISS and interprets recent experiments, for example, the CISS-driven anomalous Hall effect.

I. INTRODUCTION

Chirality induced spin selectivity (CISS) is a fascinating effect where electrons get spin polarized after propagating through chiral organic molecules like DNA [1–4]. CISS reveals an intriguing relation between the structural chirality and the electron spin or orbital [5, 6], and is promising to design novel spintronic devices using chiral molecules [7], realize enantiomers separation [8], and study the spin-selective biological process [3, 4]. Despite the debate on the microscopic mechanisms (see Ref. [9] and references therein), the chiral molecule is widely regarded a spin filter.

The CISS spin filter represents that the chiral molecule exhibits a selected transmission rate in one spin channel compared to the opposite spin, in which the preferred spin depends on the chirality. The spin filter was presumed to induce opposite spin polarization in transmitted and reflected electrons (see Fig. 1a). This scenario was further generalized to argue that a chiral molecule exhibits transient, opposite spin polarization at two ends in the charge displacement process (see Ref. [4] for review). In literature, the spin filter is frequently adopted to rationalize CISS experiments such as the magnetoresistance [10–22], anomalous Hall effect (AHE) [23, 24], and the selected chiral adsorption [8, 25]. Such a spin filter scenario is plausibly based on an elusive argument that the total spin density remains zero to preserve the net spin polarization. However, it is established that spin polarization is not necessarily conserved in transport by earlier studies on spintronics, for example, the Rashba-Edelstein effect where the current leads to net spin polarization in a nonmagnetic material [26, 27]. Therefore, this well-accepted model deserves more examination.

In this work, we point out that the present spin filter

picture violates the principle that spin current must vanish at equilibrium. We prove that both transmitted and reflected electrons present the same type of spin polarization in a generic two-terminal device, including the CISS effect. Chiral molecules play the role of a spin polarizer (Fig. 1b) rather than a spin filter, because they polarize all scattered (transmitted and reflected) electrons to the same direction, which relies on the molecule chirality and electron incident direction. The spin polarizer picture provides further understandings on CISS, especially on the CISS-driven anomalous Hall effect and the transient spin polarization of chiral molecules in dynamical chemical processes. The scope of present work is to understand the current-induced spin polarization from a nonmagnetic CISS device. We ignore the case involving magnetic electrodes in which CISS-induced magnetoresistance is commonly measured and exhibits essential features beyond the spin polarization [28–30].

II. RESULTS

A. Prohibition of equilibrium spin current

We will discuss a generic two terminal device with nonmagnetic electrodes. It is established that the equilibrium spin current is strictly forbidden between two terminals because of the time reversal symmetry [31]. In the quantum scattering problem, electrons income from the left or right to the center region and are transmitted (t from the left, t' from the right) or reflected (r from the left, r' from the right), as shown in Fig. 1. We denote the spin conductance of a scattering state i as $\sigma_i = i_{\uparrow\uparrow} - i_{\downarrow\downarrow}$ ($i = t, t', r, r'$). We note that the spin conductance is different from the ratio of spin polarization.

As shown in Fig. 1, we denote by “spin filter” the scenario that transmission and reflection have opposite spin polarization, and by “spin polarizer” the scenario that they have the same sign. In a CISS device, the 180° ro-

* binghai.yan@weizmann.ac.il

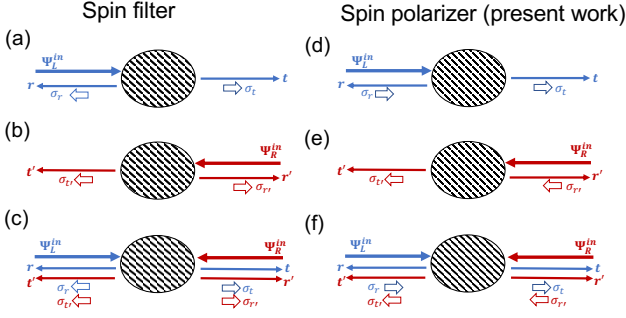


FIG. 1. Schematics of transmission and reflection in a two-terminal device. The incident wave from the left (right), Ψ_L^{in} (Ψ_R^{in}), gets scattered with transmission rate t (t') and reflection rate r (r'). The transmission and reflection exhibit spin conductance, σ_t ($\sigma_{t'}$) and σ_r ($\sigma_{r'}$), respectively. The spin filter requires that σ_t ($\sigma_{t'}$) and σ_r ($\sigma_{r'}$) have opposite signs in (a) [(b)]. In (c) electrons come from the left (Ψ_L^{in}) and right (Ψ_R^{in}) equally, represent the equilibrium state. Then, the left (r , t') and right (t , r') scattered waves carry opposite spins. Therefore, the equilibrium spin current emerges in (c), which is unphysical. In contrast, the spin polarizer leads to the same sign in σ_t ($\sigma_{t'}$) and σ_r ($\sigma_{r'}$) in (d) [(e)]. Then, the equilibrium spin current can be avoided in (f) if Eqs. 1 and 2 hold.

tation of the molecule gives rise to the same sign of spin polarization in transmission because the rotation does not change the chirality. For given chirality, the polarization direction of σ_t is locked to the transmission direction in a parallel or antiparallel way. Thus, σ_t is expected to be opposite to $\sigma_{t'}$ in sign because of opposite transmission directions. In equilibrium, electrons are equally incident from and scattered to the left and right. The spin filter presents an equilibrium spin current because left-polarized (σ_r , $\sigma_{t'}$) and right-polarized (σ_t , $\sigma_{r'}$) spins simultaneously move to the left and right, respectively, in Fig. 1c.

In contrast, the spin polarizer can avoid the spin current at equilibrium as long as the spin conductance satisfies the condition (Fig. 1f),

$$\sigma_t + \sigma_{r'} = 0 \quad (1)$$

$$\sigma_r + \sigma_{t'} = 0 \quad (2)$$

We will prove that this condition is guaranteed by the unitary property of the scattering matrix in the following.

B. Scattering matrix and spin polarization

In the two-terminal device, we define the scattering matrix in the usual notation, as the matrix relating the incoming waves, Ψ_L^{in} and Ψ_R^{in} , to the outgoing waves, Ψ_L^{out} and Ψ_R^{out} :

$$\begin{pmatrix} \Psi_L^{out} \\ \Psi_R^{out} \end{pmatrix} = S \begin{pmatrix} \Psi_L^{in} \\ \Psi_R^{in} \end{pmatrix} = \begin{pmatrix} r & t' \\ t & r' \end{pmatrix} \begin{pmatrix} \Psi_L^{in} \\ \Psi_R^{in} \end{pmatrix} \quad (3)$$

The unitary property $SS^\dagger = \mathbb{1}$ of the S -matrix leads to,

$$rr^\dagger + t't'^\dagger = \mathbb{1} \quad (4)$$

$$r'r'^\dagger + tt^\dagger = \mathbb{1} \quad (5)$$

Ψ_L^{in} and Ψ_R^{in} are incoming wave functions from the left and right leads, respectively. By assuming N independent channels in each lead, $\Psi_{L,R}^{in}$ have $2N$ dimensions because of the spin degeneracy. The density matrix ρ_i of the scattered wave (i) can be expressed as,

$$\rho_r = rr^\dagger, \rho_t = tt^\dagger, \rho_{r'} = r'r'^\dagger, \rho_{t'} = t't'^\dagger, \quad (6)$$

It is convenient to calculate the spin conductance of a specific state (i) using the corresponding density matrix (ρ_i). Denoting the transport axis as the z direction, the spin conductance is

$$\sigma_i \equiv \langle \sigma_z \rangle_i = Tr[\sigma_z \rho_i] \quad (7)$$

Combing Eqs. 4,5,6 and 7, we can derive Eqs. 1 and 2, i.e., the condition to avoid equilibrium spin current. We must stress that Eqs. 1 and 2 are generic for any two-terminal devices with nonmagnetic leads, as long as the unitarity of the S -matrix holds.

For a symmetric CISS device, the two-fold rotation symmetry requires $\sigma_t = -\sigma_{t'}$. From Eqs. 1 and 2 we obtain,

$$\sigma_t = \sigma_r = -\sigma_{t'} = -\sigma_{r'}. \quad (8)$$

A similar relation to Eq. 8 was also derived from a different scheme in Ref. [32]. In a general CISS devices beyond the two-fold symmetry constraint, we relax the above conditions to σ_t and $\sigma_{t'}$ having opposite signs. From Eqs. 1 and 2, we obtain that transmission and reflection have the same sign in spin conductance (thus also the same sign of spin polarization),

$$\sigma_t \sigma_r > 0, \quad \sigma_{t'} \sigma_{r'} > 0. \quad (9)$$

These results support the spin polarizer scenario rather than the spin filter.

More generally, the above results hold for the conductance of any operator \mathcal{O} that satisfies $Tr[\mathcal{O}] = 0$. Detailed derivations based on the outcome of the time-reversal symmetry are presented in Appendix A. For example, the orbital angular momentum operator L is such an operator, and angular momentum polarization of transmission and reflection also exhibit the same sign. In summary, the chiral molecule serve as a polarizer, rather than a filter, for spins or orbitals[5] of conducting electrons.

The above discussion holds for the coherent transport, in which the unitary condition of Eqs. 4 and 5 holds. For a dissipating system, we can include dissipation by modifying the unitarity condition, $SS^\dagger = (1 - \delta)\mathbb{1} + \epsilon A$, where δ is a uniform dissipation of all the modes and ϵA is a selective dissipation term for the different modes. The

matrix A is normalized such that its eigenvalues are no larger than 1, and ϵ controls the magnitude of selective dissipation. Following the same process as before, by using Eqs. 6 and 7 and taking the trace on the modified unitary conditions, we get:

$$\sigma_t = -\sigma_{r'} + \epsilon Tr[\sigma_z A_1] \quad \sigma_{t'} = -\sigma_r + \epsilon Tr[\sigma_z A_2] \quad (10)$$

Where A_1 is the left upper block of A and A_2 is the right lower block. We see that the uniform dissipation δ does not play a role, only the part that creates selectivity in dissipation of the different modes, and that is bound by $\epsilon Tr[\sigma_z A_1]$ and $\epsilon Tr[\sigma_z A_2]$. The trace of $\sigma_z A_i$ is no larger than $Tr[|A_i|] \leq 2N$. As there are $2N$ independent modes in each lead, we normalize the spin conductance by $2N$ in order to have $-1 \leq \sigma \leq 1$. Thus, we get:

$$|\sigma_t + \sigma_{r'}| < \epsilon \quad |\sigma_{t'} + \sigma_r| < \epsilon \quad (11)$$

Assuming $\sigma_t = -\sigma_{t'}$, we get:

$$|\sigma_t - \sigma_r| < \epsilon \quad |\sigma_{t'} - \sigma_{r'}| < \epsilon \quad (12)$$

From this, we see that if the spin conductance is larger than the magnitude of the selective dissipation term, then the conductance of transmission and reflection spin have the same sign. The intuitive explanation to why selective dissipation of modes alters the spin conductance induced by the chirality of the molecule, is that selective dissipation is an orthogonal mechanism that can theoretically polarize spin as well, for example, selective dissipation of spin down states in an unpolarized current leaves the current spin polarized in the up direction.

C. Quantum transport calculations

To examine the above analytic results, we performed Landauer-Büttiker quantum transport calculations on two-terminal CISS devices. The device is composed of a helical chain sandwiched between half-infinite linear chains, as illustrated in Fig. 2a. Each site has $p_{x,y,z}$ orbitals and two spins. Between sites, we set Slater-Koster type[33] hopping parameters to nearest neighbors. Thus, hopping parameters manifest the chirality by picking up different phases between different chiral structures[5]. We only set finite spin-orbit coupling (SOC, λ_{SOC}) at two interface sites, to represent that electrodes exhibit dominantly larger λ_{SOC} than the organic chiral molecule in a CISS device. However, our main conclusions will be independent of whether λ_{SOC} comes from the molecule or electrodes. The spin polarization in both terminals is well defined in the calculations because there, we set the SOC to zero. All the conductance calculations were performed with Kwant[34]. Parameters of the model and band structure of leads and chiral chain can be found in appendix B.

Figures 2b-c show the case of a symmetric device. The transmission and reflection are calculated for different Fermi energies, which fully agree with Eq. 8. After

violating the C_2 symmetry by setting λ_{SOC} which differ between the two interfaces (Fig. 2d-e), σ_t and σ_r ($\sigma_{t'}$ and $\sigma_{r'}$) are not equal in values, but Eqs.1, 2 and 9 are always valid.

Figures 2d-e already demonstrate sensitive dependence of the spin conductance on SOC. Furthermore, we set an extreme example with $\lambda_{SOC,L} = 0$ and $\lambda_{SOC,R} = 1$ in Fig. 3 and calculate both the spin and orbital (L) conductance here. One striking feature is that σ_r and $\sigma_{t'}$ are diminished in amplitude while $\sigma_{r'}$ and σ_t are still significant. Because the orbital is less sensitive to λ_{SOC} , the orbital conductance $L_{r,t,r',t'}$ exhibits a large amplitude and satisfies,

$$L_t + L_{r'} = 0, \quad L_r + L_{t'} = 0 \quad (13)$$

$$L_t L_{r'} > 0, \quad L_{t'} L_r > 0 \quad (14)$$

One intuitive picture is that electrons get orbital polarized in the chiral molecule and the interface SOC converts the orbital polarization to spin polarization. For example, $\lambda_{SOC,R}$ converts large L_t ($L_{r'}$) to σ_t ($\sigma_{r'}$) while there is no $\lambda_{SOC,L}$ to induce σ_r ($\sigma_{t'}$) from L_r ($L_{t'}$). In addition, the tiny amplitude of σ_r ($\sigma_{t'}$) at some energies is induced by the weak interface orbital-spin conversion due to $\lambda_{SOC,R}$.

In the orbital-spin conversion, we observe a counter-intuitive effect, that the transmitted/reflected spin conductance remains the same when reversing the sign of λ_{SOC} (see Appendix Fig. A2a and A2b). It becomes

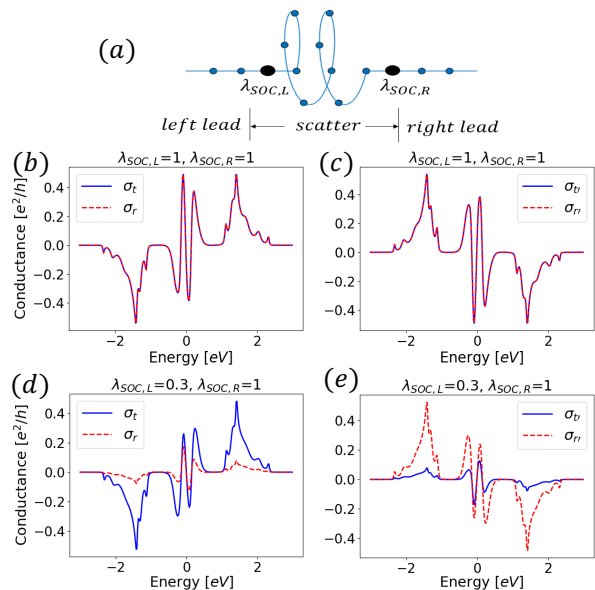


FIG. 2. (a) Generic structure of the CISS device, including the leads and interface. (b)-(c) Calculated spin conductance of t, r, t', r' in a C_2 symmetric system at different Fermi energies. (d)-(e) The same spin conductance in a C_2 -symmetry-breaking system by differentiating $\lambda_{SOC,L}$ and $\lambda_{SOC,R}$. $\lambda_{SOC,L/R}$ represents the value of spin-orbit coupling at the left/right interface.

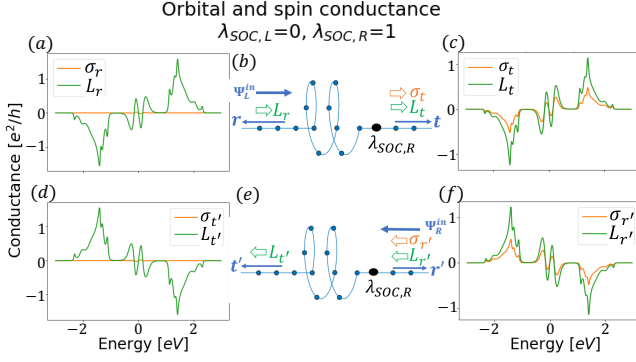


FIG. 3. Orbital and spin conductance in a system where C_2 symmetry is broken by having SOC only on the right side. (a)-(c) Orbital and spin conductance of r and t : Current coming from the left gets orbital polarized along the chain, then, the orbital current is converted to spin current by the SOC atom. (d)-(f) Orbital and spin conductance of r' and t' : Current coming from the right hits the SOC atom before getting orbital polarized, so it passes unaltered into the chain, where it gets orbital polarized, after which it passes to the left lead only orbital polarized.

rational when considering that SOC connects states with the same total angular momentum $J_z = L_z \pm S_z$ as a scattering potential. No matter the sign of the SOC, the allowed transitions between the chiral chain and electrode are dictated by non-zero matrix elements of the SOC Hamiltonian ("selection rules"). Suppose the orbital polarization in the chiral chain will be in favor of $L_z = +1$ and equal probability for $S_z = \pm \frac{1}{2}$. Direct calculation of these matrix elements shows that the allowed transitions are:

$$\begin{aligned} |L_z = 1, S_z = \frac{1}{2}\rangle &\rightarrow |L_z = 1, S_z = \frac{1}{2}\rangle \\ |L_z = 1, S_z = -\frac{1}{2}\rangle &\rightarrow |L_z = 1, S_z = -\frac{1}{2}\rangle, \\ |L_z = 0, S_z = \frac{1}{2}\rangle & \end{aligned}$$

We can see that these selection rules allow the positive orbital polarization to convert spin states, from down to up, by trading angular momentum between orbital and spin, while a up-down-down conversion of spins is not allowed. Thus, the positive orbital polarization leads to the positive spin polarization, when scattered by the SOC site. Similarly, a negative orbital polarization generates negative spin polarization. The orbital and spin relation is shown by the same sign between σ_t and L_t (also $\sigma_{r'}$ and $L_{r'}$) in Fig. 3.

D. Discussion on experiments

As discussed above, the direction of the spin polarization is determined by the current direction and molecule

chirality while the magnitude of spin polarization depends on the local SOC. This observation provides insights on the CISS-induced transient spin polarization of chiral molecules. In chemical reactions or surface adsorption, it is commonly argued in literature[8, 25, 35–37] that the instantaneous charge displacement leads to opposite spin polarization at both ends of a chiral molecule (as illustrated in Fig. 4a-b) by assuming the spin filter scenario. Following the picture of spin polarizer, we expect that both ends exhibit the same sign of spin polarization (see Fig. 4c). If the organic chiral molecule is isolated far from a strong SOC region (e.g., a substrate or electrode), the magnitude of spin polarization may be negligible because of weak SOC. If the molecule is close to a heavy metal surface (Fig. 4d), the interface region may develop substantial spin polarization. Additionally, such transient spin polarization may vanish soon after the spin lifetime when the system approaches equilibrium.

It is noteworthy that the spin polarizer mechanism gets more rational when one considers the previous AHE experiments [23, 24]. When the top gate ejects/extracts electrons through a layer of chiral molecules into/out of doped-GaAs or GaN, the magnetization was induced in the doped semiconducting layer and monitored by the AHE. Switching the gate voltage was found to reverse the sign of induced magnetization in the semiconductor. The spin polarizer naturally indicates opposite spin polarizations in the semiconductor after reversing the tunnelling direction for the given chirality (Fig. 1d-e), which is consistent with experiments. However, the spin filter scenario would indicate no sign change in the semiconductor side (Fig. 1a-b) after switching the gate voltage.

III. SUMMARY

In summary, we proposed that the spin polarizer model is more rational than the spin filter for the chiral molecule in the CISS device. Here, the transmitted and reflected

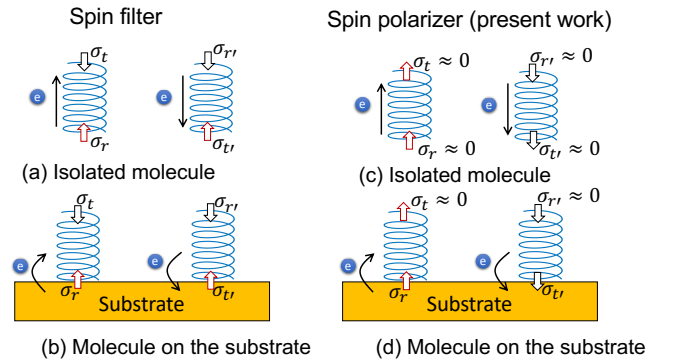


FIG. 4. Transient spin polarization in (a)&(c) the isolated chiral molecule and (b)&(d) a chiral molecule on the surface. The instantaneous charge redistribution is indicated by the black arrow. The spin conductance σ_i represents the transient spin polarization and is defined in the same way as Fig. 1.

electrons exhibit the same sign in spin polarization as a leading order effect. This scenario provides deeper understanding on the CISS-driven spin polarization and alternative explanations on the induced AHE and transient spin polarization. The spin polarizer (filter) leads to opposite (same) spin polarization direction in a given electrode when reversing the current direction. Thus, the current-direction-specific spin polarization provides a smoking-gun evidence to verify the spin polarizer effect in experiments.

ACKNOWLEDGMENTS

We thank helpful discussions with Ron Naaman. B.Y. acknowledges the financial support by the European Research Council (ERC Consolidator Grant “NonlinearTopo”, No. 815869) and the MINERVA Stiftung with the funds from the BMBF of the Federal Republic of Germany. N.P. was supported by the NRF of Korea government (MSIT)(No. NRF-2019R1A2C2089332).

-
- [1] K. Ray, S. P. Ananthavel, D. H. Waldeck, and R. Naaman, *Science* **283**, 814 (1999).
- [2] B. Gohler, V. Hamelbeck, T. Z. Markus, M. Kettner, G. F. Hanne, Z. Vager, R. Naaman, and H. Zacharias, *Science* **331**, 894 (2011).
- [3] R. Naaman and D. H. Waldeck, *The Journal of Physical Chemistry Letters* **3**, 2178 (2012).
- [4] R. Naaman, Y. Paltiel, and D. H. Waldeck, *Nature Reviews Chemistry* **3**, 250 (2019).
- [5] Y. Liu, J. Xiao, J. Koo, and B. Yan, *Nature Materials* **6**, 638–644 (2021).
- [6] J. Gersten, K. Kaasbjerg, and A. Nitzan, *The Journal of Chemical Physics* **139**, 114111 (2013), 1306.4904.
- [7] S.-H. Yang, R. Naaman, Y. Paltiel, and S. S. Parkin, *Nature Reviews Physics* **3**, 328 (2021).
- [8] K. Banerjee-Ghosh, O. Ben Dor, F. Tassinari, E. Capua, S. Yochelis, A. Capua, S.-H. Yang, S. S. Parkin, S. Sarkar, L. Kronik, *et al.*, *Science* **360**, 1331 (2018).
- [9] F. Evers, A. Aharony, N. Bar-Gill, O. Entin-Wohlman, P. Hedegård, O. Hod, P. Jelinek, G. Kamieniarz, M. Lemesko, K. Michaeli, *et al.*, *Advanced Materials* **34**, 2106629 (2022).
- [10] Z. Xie, Z. Xie, T. Z. Markus, S. R. Cohen, Z. Vager, R. Gutierrez, and R. Naaman, *Nano letters* **11**, 4652 (2011).
- [11] M. Kettner, B. Gohler, H. Zacharias, D. Mishra, V. Kiran, R. Naaman, C. Fontanesi, D. H. Waldeck, S. Sek, J. Pawaowski, and J. Juhaniwicz, *The Journal of Physical Chemistry C* **119**, 14542 (2015).
- [12] R. Naaman and D. H. Waldeck, *Annu. Rev. Phys. Chem* **66**, 263 (2015).
- [13] V. Kiran, S. P. Mathew, S. R. Cohen, I. H. Delgado, J. Lacour, and R. Naaman, *Advanced Materials* **28**, 1957 (2016).
- [14] H. Al-Bustami, G. Koplovitz, D. Primc, S. Yochelis, E. Capua, D. Porath, R. Naaman, and Y. Paltiel, *Small* **14**, 1801249 (2018).
- [15] V. Varade, T. Markus, K. Vankayala, N. Friedman, M. Sheves, D. H. Waldeck, and R. Naaman, *Physical Chemistry Chemical Physics* **20**, 1091 (2018).
- [16] T. Liu, X. Wang, H. Wang, G. Shi, F. Gao, H. Feng, H. Deng, L. Hu, E. Lochner, P. Schlottmann, S. von Molnár, Y. Li, J. Zhao, and P. Xiong, *ACS Nano* **14**, 15983 (2020).
- [17] H. Lu, J. Wang, C. Xiao, X. Pan, X. Chen, R. Brunecky, J. J. Berry, K. Zhu, M. C. Beard, and Z. V. Vardeny, *Science Advances* **5**, eaay0571 (2019).
- [18] D. M. Stemer, J. M. Abendroth, K. M. Cheung, M. Ye, M. S. E. Hadri, E. E. Fullerton, and P. S. Weiss, *Nano Letters* **20**, 1218 (2020).
- [19] S. Ghosh, S. Mishra, E. Avigad, B. P. Bloom, L. T. Baczewski, S. Yochelis, Y. Paltiel, R. Naaman, and D. H. Waldeck, *The Journal of Physical Chemistry Letters* **11**, 1550 (2020).
- [20] H. Lu, C. Xiao, R. Song, T. Li, A. E. Maughan, A. Levin, R. Brunecky, J. J. Berry, D. B. Mitzi, V. Blum, *et al.*, *Journal of the American Chemical Society* **142**, 13030 (2020).
- [21] A. K. Mondal, M. D. Preuss, M. L. Sleczkowski, T. K. Das, G. Vantomme, E. Meijer, and R. Naaman, *Journal of the American Chemical Society* **143**, 7189 (2021).
- [22] Y. Lu, Q. Wang, R. He, F. Zhou, X. Yang, D. Wang, H. Cao, W. He, F. Pan, Z. Yang, *et al.*, *Angewandte Chemie International Edition* **60**, 23578 (2021).
- [23] E. Z. Smolinsky, A. Neubauer, A. Kumar, S. Yochelis, E. Capua, R. Carmieli, Y. Paltiel, R. Naaman, and K. Michaeli, *The journal of physical chemistry letters* **10**, 1139 (2019).
- [24] S. Mishra, A. K. Mondal, E. Z. B. Smolinsky, R. Naaman, K. Maeda, T. Nishimura, T. Taniguchi, T. Yoshida, K. Takayama, and E. Yashima, *Angewandte Chemie* **132**, 14779 (2020).
- [25] F. Tassinari, J. Steidel, S. Paltiel, C. Fontanesi, M. Lahav, Y. Paltiel, and R. Naaman, *Chemical Science* **10**, 5246 (2019).
- [26] V. M. Edelstein, *Solid State Communications* **73**, 233 (1990).
- [27] J. Sánchez, L. Vila, G. Desfonds, S. Gambarelli, J. Attané, J. De Teresa, C. Magén, and A. Fert, *Nature communications* **4**, 1 (2013).
- [28] S. Dalum and P. Hedegård, *Nano Letters* **19**, 5253 (2019).
- [29] X. Yang, C. H. van der Wal, and B. J. van Wees, *Nano Letters* **20**, 6148 (2020).
- [30] J. Xiao and B. Yan, *arXiv preprint arXiv:2201.03623* (2022).
- [31] A. A. Kiselev and K. W. Kim, *Phys. Rev. B* **71**, 12974–12980 (2005).
- [32] X. Yang, C. H. v. d. Wal, and B. J. v. Wees, *Physical Review B* **99**, 024418 (2019), 1810.02662.
- [33] J. C. Slater and G. F. Koster, *Phys. Rev.* **94**, 1498 (1954).
- [34] C. W. Groth, M. Wimmer, A. R. Akhmerov, and X. Waintal, *New Journal of Physics* **16**, 063065 (2014).
- [35] R. Naaman, D. H. Waldeck, and Y. Paltiel, *Applied Physics Letters* **115**, 133701 (2019).
- [36] A. Ziv, A. Saha, H. Alpern, N. Sukenik, L. T. Baczewski, S. Yochelis, M. Reches, and Y. Paltiel, *Advanced Materials* **31**, 1904206 (2019).

- [37] K. Santra, Q. Zhang, F. Tassinari, and R. Naaman, *The Journal of Physical Chemistry B* **123**, 9443 (2019).

Appendix A: Derivation of Polarization Equality Between Transmitted and Reflected States

Here, we shall show that in a two terminal system with no dissipation and leads that respect time reversal symmetry, the polarization of transmitted and reflected currents with respect to a general traceless operator, \mathcal{O} , is the same. An incoming or outgoing state from the left or right has $2N$ components, corresponding to N orbitals, each 2-fold degenerate in spin.

In the density matrix formalism, the relation between an incoming state and an outgoing state is given by:

$$\rho_{out} = S\rho_{in}S^\dagger = \begin{pmatrix} r & t' \\ t & r' \end{pmatrix} \begin{pmatrix} \rho_L^{in} & 0 \\ 0 & \rho_R^{in} \end{pmatrix} \begin{pmatrix} r^\dagger & t'^\dagger \\ t'^\dagger & r'^\dagger \end{pmatrix} \quad (\text{A1})$$

Carrying out the matrix multiplication yields the outgoing states in the left and right:

$$\begin{pmatrix} \rho_L^{out} & * \\ * & \rho_R^{out} \end{pmatrix} = \begin{pmatrix} r\rho_L^{in}r^\dagger + t'\rho_L^{in}t'^\dagger & * \\ * & r'\rho_R^{in}r'^\dagger + t\rho_R^{in}t^\dagger \end{pmatrix} \quad (\text{A2})$$

When current is incoming only from the left, $\rho_R^{in} = 0_{2N \times 2N}$. In addition, under the assumption of an incoherent sum of modes incoming from the left, $\rho_L^{in} = \mathbb{1}_{2N \times 2N}$. Plugging into the above equation:

$$\rho_L^{out} = rr^\dagger \equiv \rho_r \quad \rho_R^{out} = tt^\dagger \equiv \rho_t \quad (\text{A3})$$

Similarly, when current is incoming only from the right:

$$\rho_R^{out} = r'r'^\dagger \equiv \rho_{r'} \quad \rho_L^{out} = t't'^\dagger \equiv \rho_{t'} \quad (\text{A4})$$

From the unitarity condition of the density matrix in eq. (4)

$$\rho_r + \rho_{t'} = \mathbb{1} \quad (\text{A5})$$

Multiplying by \mathcal{O} and taking the trace:

$$\text{Tr}[\mathcal{O}\rho_r] + \text{Tr}[\mathcal{O}\rho_{t'}] = \text{Tr}[\mathcal{O}] \quad (\text{A6})$$

As the trace of \mathcal{O} is zero, and using the generalized form of eq. (7) for expectation value, $\text{Tr}[\mathcal{O}\rho_i] = \langle \mathcal{O} \rangle_i$, we obtain:

$$\mathcal{O}_r + \mathcal{O}_{t'} = 0 \quad (\text{A7})$$

Similarly, using the second unitary relation in eq. (5), we obtain:

$$\mathcal{O}_{r'} + \mathcal{O}_t = 0 \quad (\text{A8})$$

When these outcomes are combined with the selectivity inherent to the C_2 symmetric system, $\mathcal{O}_t = -\mathcal{O}_{t'}$, we obtain:

$$\mathcal{O}_r = \mathcal{O}_t = -\mathcal{O}_{t'} = -\mathcal{O}_{r'} \quad (\text{A9})$$

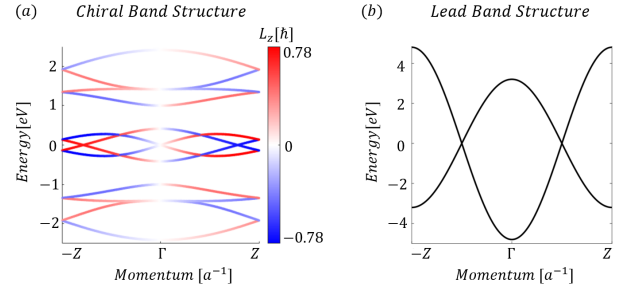


FIG. A1. (a) Band structure of chiral molecule in the infinite chain form. The blue and red colors represent the orbital projection. (b) Band structure of the lead.

Appendix B: Parameters of Model and Band Structure

In the model we work with electrons in the basis of the of the 3 p orbitals and the up and down states of spin half: $\{|p_x\rangle, |p_y\rangle, |p_z\rangle\} \otimes \{|\uparrow\rangle, |\downarrow\rangle\}$. The parameters will all be given in units of eV . In addition, they will be shown as an outer product of 3×3 matrices in the p orbital basis, with 2×2 matrices in the spinor basis.

In the left and right lead, we use the nearest neighbor hopping matrix:

$$t_{lead} = \begin{pmatrix} -2.4 & 0 & 0 \\ 0 & -2.4 & 0 \\ 0 & 0 & 1.6 \end{pmatrix} \otimes \mathbb{1}_{2 \times 2} \quad (\text{B1})$$

The on-site matrix term of the left and right lead is set to zero. The band structure of the leads can be seen in Fig. (A1b).

The interface between the left lead and the chiral molecule contains one atom. The hopping from the lead to this atom is given by the above hopping matrix (B1), and the hopping into the chiral molecule is given by the

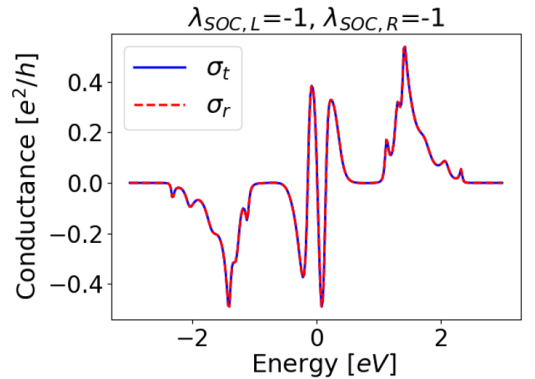


FIG. A2. Spin polarization of t and r for negative SOC on both sides. Same sign of polarization as positive SOC.

following hopping matrix:

$$t_{SOC} = \begin{pmatrix} -1.5 & 0 & 0 \\ 0 & -1.5 & 0 \\ 0 & 0 & 1 \end{pmatrix} \otimes \mathbb{1}_{2 \times 2} \quad (\text{B2})$$

The onsite term of the atom in the interface is the SOC Hamiltonian:

$$h_{SOC} = \lambda_{SOC,L} \sum_{i=x,y,z} l_i \otimes \sigma_i \quad (\text{B3})$$

Where σ_i are the three Pauli matrices and l_i are the (unitless) angular momentum operators as 3×3 matrices in the p orbital basis. $\lambda_{SOC,L}$ denotes the spin-orbit coupling constant, L indicates that this is the interface with the left lead.

For the interface between the chiral molecule and the right lead, we use the exact same model, we only change the spin-orbit coupling constant $\lambda_{SOC,R}$.

The hopping in the chiral molecule is nearest neighbors and is given by the following matrix:

$$t_{chiral,ij} = \begin{pmatrix} t_{xx} & t_{xy} & t_{xz} \\ t_{yx} & t_{yy} & t_{yz} \\ t_{zx} & t_{zy} & t_{zz} \end{pmatrix} \otimes \mathbb{1}_{2 \times 2} \quad (\text{B4})$$

$$\begin{aligned} t_{xx,ij} &= t_\pi \sin^2 \phi_{ij} + \cos^2 \phi_{ij} (t_\sigma \sin^2 \theta_{ij} + t_\pi \cos^2 \theta_{ij}) \\ t_{yy,ij} &= t_\pi \cos^2 \phi_{ij} + \sin^2 \phi_{ij} (t_\sigma \sin^2 \theta_{ij} + t_\pi \cos^2 \theta_{ij}) \\ t_{zz,ij} &= t_\sigma \cos^2 \theta_{ij} + t_\pi \sin^2 \theta_{ij} \\ t_{xy,ij} &= t_{yx} = \sin \phi_{ij} \cos \phi_{ij} (t_\sigma \sin^2 \theta_{ij} - t_\pi \cos^2 \theta_{ij}) \\ t_{xz,ij} &= t_{zx} = \cos \phi_{ij} \sin \theta_{ij} \cos \theta_{ij} (t_\sigma - t_\pi) \\ t_{yz,ij} &= t_{zy} = \sin \phi_{ij} \sin \theta_{ij} \cos \theta_{ij} (t_\sigma - t_\pi) \end{aligned}$$

Where θ_{ij} and ϕ_{ij} are the spherical coordinates of site j with respect to site i . In our model, we use a helix with a C_4 -skew symmetry, such that ϕ_{ij} can adopt the angles $\frac{\pi}{8}, \frac{\pi}{8} + \frac{\pi}{2}, \frac{\pi}{8} + \frac{2\pi}{8}, \frac{\pi}{8} + \frac{3\pi}{8}$ and $\theta_{ij} = \pm \frac{\pi}{4}$. In the model, the chiral molecule contains 8 atoms and $t_\pi = -0.5eV$, $t_\sigma = 1.5eV$. The onsite terms in the chiral molecule is set to zero. The band structure of the chiral chain can be seen in Fig. (A1a).